

# Spontaneous symmetry and antisymmetry breaking in a ring with two potential barriers

Hidetsugu Sakaguchi<sup>1</sup>, Boris A. Malomed<sup>2,3a</sup>, and T. J. Taiwo<sup>4</sup>

<sup>1</sup>*Department of Applied Science for Electronics and Materials,  
Interdisciplinary Graduate School of Engineering Sciences,  
Kyushu University, Kasuga, Fukuoka 816-8580, Japan*

<sup>2</sup>*Department of Physical Electronics, School of Electrical Engineering,  
Faculty of Engineering, and Center for Light-Matter Interaction,  
Tel Aviv University, P.O. Box 39040 Tel Aviv, Israel*

<sup>3</sup>*Instituto de Alta Investigación, Universidad de Tarapacá, Casilla 7D, Arica, Chile and*

<sup>4</sup>*Department of Physics, United Arab Emirates University. Al Ain, United Arab Emirates*

We propose a fundamental setup for the realization of spontaneous symmetry breaking (SSB) and spontaneous antisymmetry breaking (SASB) in the framework of the nonlinear Schrödinger equation with the self-attractive and repulsive cubic term, respectively, on a one-dimensional ring split in two mutually symmetric boxes by delta-functional potential barriers, placed at opposite points. The system is relevant to optics and BEC. The spectrum of the linearized system is found in analytical and numerical forms. SSB and SASB are predicted by dint of the variational approximation, and studied in the numerical form. A particular stable solution, which demonstrates strong asymmetry, is found in an exact form. In the system with the attractive nonlinearity, the SSB of the symmetric ground state is initiated by the modulational instability. It creates stationary asymmetric states through a supercritical bifurcation. In the self-repulsive system, SASB makes the lowest antisymmetric excited state unstable, transforming it into an antisymmetry-breaking oscillatory mode.

Spontaneous symmetry breaking (SSB) is a fundamental aspect of complexity in a broad range of nonlinear dynamical systems. While eigenstates of linear systems with intrinsic symmetry (which may be typically represented by a double-well potential, or by a symmetric pair of subsystems coupled by linear mixing) exactly follow this intrinsic structure, featuring either symmetry or antisymmetry with respect to it (in particular, this is a fundamental feature of quantum mechanics, where the ground state (GS) and all excited states (ESs) of even orders precisely follow the symmetry of the underlying potential, while the first ES and all others of odd orders are antisymmetric), a sufficiently strong self-attractive nonlinearity may fundamentally change the situation by destabilizing the symmetric GS and replacing it by a stable *asymmetric* one. The self-repulsive nonlinearity does not break the symmetry of the GS, but it may destabilize the lowest antisymmetric ES. The latter effect may be called spontaneous antisymmetry breaking (SASB). The SSB/SASB phenomenology was studied in detail theoretically and demonstrated experimentally in many settings, especially in nonlinear optics and photonics and in quantum matter (primarily, ultracold atomic gases in the state of the Bose-Einstein condensation (BEC)). Nevertheless, it remains a relevant objective to explore SSB and SASB in the most basic settings, where the corresponding phase transitions (alias bifurcations) may be demonstrated in a transparent form. This work introduces a basic setting which was not studied before, *viz.*, a ring split in two mutually symmetric boxes by a pair of identical narrow potential barriers set at diametrically opposite points and represented by delta-functions. The model is represented by the nonlinear Schrödinger equation with the pair of delta-functional repulsive potentials and self-attractive or repulsive cubic nonlinearity. In terms of the physical realization, the model is relevant to optics and BEC alike. The relative simplicity of the model makes it possible to develop a systematic analytical consideration, by means of the variational approximation, which is performed parallel to a comprehensive numerical analysis. In addition to that, a particular exact analytical solution is found. Both the analytical and numerical results reveal the *supercritical bifurcation* representing the SSB in the case of the attractive nonlinearity. The bifurcation destabilizes the symmetric GS, replacing it by an explicitly found asymmetric one. In the case of the self-repulsion, the SASB destabilizes the lowest antisymmetric ES. However, no stationary state with broken antisymmetry is found in the latter case; instead, the basic outcome of the SASB is replacement of the lowest ES by a breather, i.e., a robust oscillatory state with broken antisymmetry.

---

<sup>a</sup> The corresponding author; e-mail malomedtauex.tau.ac.il

## I. INTRODUCTION

Symmetry is a profound property of many physical systems, therefore spontaneous symmetry breaking (SSB) in nonlinear systems is a fundamental phenomenon with well-known manifestations in optics and photonics, matter waves (Bose-Einstein condensates, BECs), and other fields [1]. Following early theoretical works [2, 3], the SSB phenomenology was studied in detail theoretically in dual-core optical fibers (alias nonlinear couplers), especially as concerns its realization for solitons [4]–[16], see also an early review [18] and an updated one [19]. These theoretical models are based on linearly-coupled nonlinear Schrödinger (NLS) equations. The experimental demonstration of SSB and inter-core switching for solitons in dual-core fibers was reported essentially later [17]. Subsequently, this effect was predicted in photonic lattices (where it was also realized in the experiment) [20], see also Refs. [22] and [24], metamaterials [25], and dielectric resonators [26]. It was also experimentally demonstrated in coupled lasers [27–29]. In the latter case, SSB happens in dissipative nonlinear photonic systems, that may be modeled by linearly coupled complex Ginzburg-Landau equations [31].

Systems with parity-time ( $\mathcal{PT}$ ) symmetry represent the border between conservative and dissipative ones. Peculiarities of the spontaneous breaking of the  $\mathcal{PT}$  symmetry were analyzed theoretically [32–37] and demonstrated experimentally [38]. Most recently, SSB of solitons was analyzed for linearly coupled systems of NLS equations with fractional diffraction, that can be implemented in appropriately designed optical cavities [39]. In the context of BEC, SSB and related Josephson oscillations were predicted [40]–[45] and experimentally demonstrated [46] in condensates (as well as in other setups using cold atoms [47]) loaded in double-well potential traps. SSB of solitons was also studied in systems of coupled Korteweg – de Vries equations, which may be realized in fluid dynamics [48]. Manifestations of SSB were predicted as well in completely different physical settings, such as an ensemble of self-propelled particles [49].

The SSB driven by the self-attractive (focusing) nonlinearity leads to destabilization of the system’s spatially symmetric ground state (GS) and its replacement by a GS featuring a stationary asymmetric spatial structure. Under the action of the repulsive (defocusing) nonlinearity, the symmetric GS always remains stable, but the lowest excited state (ES), which is spatially antisymmetric in linear systems, may be destabilized if the self-repulsion is strong enough, which leads to the effect of the spontaneous antisymmetry breaking (SASB) [50, 51].

It is relevant to stress that the SSB concept considered in the above-mentioned works is completely different from what is also called SSB in the field theory [52–55], where it is the basis of the Higgs mechanism responsible for the creation of masses of particles [56–58].

The theoretical analysis of SSB is based on numerical methods, which may be efficiently combined with the analytical approach in the form of the variational approximation (VA) [6, 7, 14, 22, 44, 50, 59]. In this connection, it is relevant to introduce the most basic models, which make it possible to explore the SSB phenomenology in a transparent form. In particular, Ref. [60] proposed a one-dimensional (1D) NLS equation for the complex wave field  $u(x)$ , with the self-attractive cubic nonlinearity represented by a pair of delta-functions,  $[\delta(x + a/2) + \delta(x - a/2)]|u|^2u$ , with separation  $a$  between them. This model makes it possible to analyze the SSB in an exact analytical form. Also natural is to consider a 1D ring with the attractive nonlinearity concentrated at a pair of diametrically opposite points [61]. It was found that the latter model does not give rise to SSB if the spatial structure of the nonlinearity is represented by ideal delta-functions; nevertheless, the SSB takes place if the delta-functions are replaced by Gaussian profiles of a finite width [61].

While the ring with the self-attractive nonlinearity concentrated at two opposite points seems as a rather “exotic” (although physically possible [62]) configuration, in this work we aim to introduce a more natural setting based on a ring which is split in two mutually symmetric boxes (half-rings) by the linear repulsive potential represented by two delta-functions placed at diametrically opposite points. With the usual uniform self-focusing or defocusing nonlinearity, the respective NLS equation takes the form of

$$i\frac{\partial u}{\partial z} + \frac{1}{2}\frac{\partial^2 u}{\partial x^2} + \sigma|u|^2u = \epsilon \left[ \delta\left(x + \frac{\pi}{2}\right) + \delta\left(x - \frac{\pi}{2}\right) \right] u, \quad (1)$$

where  $\epsilon > 0$  is the strength of the potential barriers that split the ring. This equation is written in the form adopted in optics, with propagation distance  $z$  playing the role of the evolutionary variable [63], while the coordinate  $x$  runs along the ring, taking values

$$-\pi \leq x \leq +\pi \quad (2)$$

and imposing the periodic boundary conditions

$$u(x = -\pi) \equiv u(x = +\pi), \quad \frac{\partial u}{\partial x}(x = -\pi) \equiv \frac{\partial u}{\partial x}(x = +\pi). \quad (3)$$

Further, coefficients  $\sigma = +1$  and  $-1$  correspond, respectively, to the focusing (attractive) and defocusing (repulsive) sign of the nonlinearity in Eq. (1). Stationary solutions to Eq. (1) with real propagation constant  $k$  are looked for below in the usual form,  $u(x, t) = \exp(ikz)U(x)$ , where real function  $U(x)$  satisfies the stationary real equation,

$$-kU + \frac{1}{2} \frac{d^2 U}{dx^2} + \sigma U^3 = \epsilon \left[ \delta \left( x + \frac{\pi}{2} \right) + \delta \left( x - \frac{\pi}{2} \right) \right] U. \quad (4)$$

The repulsive potential in the form of the single delta-function may introduce SSB if it is placed at the midpoint,  $x = 0$ , of an infinitely deep potential box of a finite size  $a$ , which is described by the NLS equation with zero boundary conditions at points  $x = \pm a/2$  [64, 65]. Note that the box potentials, induced by means of an optical technique, are available in experiments with BEC [69].

The split-ring model, based on Eqs. (1)-(3), admits straightforward interpretations in terms of optics and matter waves alike. In the former case, Eq. (1) governs the propagation of light along a cylindrical surface (in particular, in hollow fibers and waveguides [66–68]). In this case, the potential barriers represent narrow strips of a material with a lower refractive index, running along the waveguide. In the application to matter waves, Eq. (1), with  $z$  replaced by time  $t$ , is the scaled Gross-Pitaevskii equation which governs the evolution of the mean-field wave function  $u(x, t)$  of BEC loaded in a toroidal trap. Such setups were created in experiments, combining magnetic, optical, and radiofrequency trapping potentials [70–73]. The narrow potential barriers in the corresponding ring configuration can be induced by a blue-detuned optical sheet cutting the torus, which has been realized in the experiment as well [78].

The following presentation is arranged as follows. First, the spectrum of the linearized version of Eq. (1) (with  $\sigma = 0$ ) is presented in Section 2. In the framework of the full nonlinear model, the SSB and SASB effects are studied, severally, for nonlinear states which originate from the spatially even GS and lowest spatially odd ES of the linear spectrum. Namely, SSB of the GS, caused by the action of the self-focusing ( $\sigma = +1$  in Eq. (1)), is addressed in Section 3, and SASB of the lowest ES under the action of the self-defocusing ( $\sigma = -1$ ) is considered in Section 4. The SSB is illustrated, first, by a particular exact analytical solution. Then, generic configurations produced by the SSB and their dynamics (including stability) are studied, in parallel, by means of the analytical VA and systematically employed numerical methods, which demonstrates good accuracy of the VA (in addition, an analytical approximation for large  $\epsilon$  is developed too). In the case of the self-focusing nonlinearity we identify the SSB bifurcation as one of the forward (alias supercritical [74, 75]) type. Past the bifurcation point, the emerging state with the broken symmetry is stable, while the symmetric one develops instability which initiates oscillatory dynamics, that features periodically recurring dynamical symmetry breaking. The instability combines features of SSB and modulational instability (MI), which is well known in 1D systems with the cubic self-focusing [63, 76, 77].

On the other hand, the variational and numerical analysis of SASB demonstrates that, past the point of the destabilization of the lowest ES, no stationary states with broken antisymmetry emerge. Instead, the simulations demonstrate establishment of a robust antisymmetry-breaking oscillatory state. The paper is concluded by Section 5.

## II. THE SPECTRUM OF THE LINEAR SYSTEM

The linearized form of Eq. (4),

$$-kU = -\frac{1}{2} \frac{d^2 U}{dx^2} + \epsilon \left[ \delta \left( x + \frac{\pi}{2} \right) + \delta \left( x - \frac{\pi}{2} \right) \right] U, \quad (5)$$

takes the form of the stationary quantum-mechanical Schrödinger equation with the repulsive delta-functional potential barriers and formal energy eigenvalue  $-k$ . The effect of the barriers amounts to the jump of the derivative of  $U(x)$  at points  $x = \pm\pi/2$ , while  $U(x)$  itself is continuous at these points:

$$\frac{dU}{dx} \left( x = \pm\frac{\pi}{2} + 0 \right) - \frac{dU}{dx} \left( x = \pm\frac{\pi}{2} - 0 \right) = 2\epsilon U \left( x = \pm\frac{\pi}{2} \right). \quad (6)$$

To produce numerical solutions, the delta-functions were replaced, as usual, by narrow Gaussians, with width  $\Delta x = 0.01$ .

Eigenstates of Eq. (5) may be defined as ones which are odd or even with respect to the positions of the delta-functions,  $x = \pm\pi/2$ . In the former cases, these are

$$U_{\text{odd}}(x) = U_0 \sin \left( \sqrt{-2k} \left( x + \frac{\pi}{2} \right) \right), \quad (7)$$

with arbitrary amplitude  $U_0$ . Because  $U_{\text{odd}}(x)$  vanishes at  $x = \pm\pi/2$ , the delta-functional potential barriers produce no effect on these eigenstates, hence the respective spectrum of eigenvalues  $k$  is the same as in the free-space ring,

determined solely by the periodicity conditions (3):

$$k_{\text{odd}} = -(n+1)^2/8, \quad n = 1, 3, 5, \dots, \quad (8)$$

where the odd quantum number  $n$  is the ES order.

The eigenstates which are even with respect to  $x = \pm\pi/2$  are naturally looked for, at  $|x| \neq \pi/2$ , as

$$U(x) = U_0 \cos\left(\sqrt{-2k}\left|x + \frac{\pi}{2}\right| + \delta\right), \quad (9)$$

where eigenvalue  $-k$  is positive (in the presence of the repulsive potential, energy eigenvalues of the linear Schrödinger equation may be, obviously, only positive), and  $\delta$  is a phase shift which should be found along with  $k$ . Note that, while the symmetry of expression (8) with respect to  $x = -\pi/2$  is obvious, the symmetry with respect to  $x = +\pi/2$  follows from the fact that the coordinate takes values in interval (2) (i.e., formal values  $x_{\text{formal}} = \pi + y$ , with  $0 < y < \pi$ , are replaced by actual ones,  $x_{\text{formal}} \rightarrow x = x_{\text{formal}} - 2\pi \equiv -(\pi - y)$ ).

The substitution of  $U(x)$  from Eq. (9) in jump conditions (6) leads to equations

$$\tan \delta = -\frac{\varepsilon}{\sqrt{-2k}}, \quad (10)$$

$$\tan\left(\sqrt{-2k}\pi + \delta\right) = \frac{\varepsilon}{\sqrt{-2k}}. \quad (11)$$

Then, substituting  $\delta = -\arctan(\varepsilon/\sqrt{-2k})$ , which follows from Eq. (10), in Eq. (11) leads to a transcendental equation which determines eigenvalues of the propagation constant  $k$ :

$$\sqrt{-2k}\pi - 2\arctan\left(\frac{\varepsilon}{\sqrt{-2k}}\right) = \frac{\pi}{2}n, \quad n = 0, 2, 4, 6, \dots, \quad (12)$$

where  $n$  is the even quantum number, whose value 0 corresponds to the GS, while other values define the number of the respective even ESs. In the general case, Eq. (12) must be solved numerically. An approximate solution can be found in the case of weak potential barriers,  $\varepsilon \ll 1$ :

$$k_{\text{small } \varepsilon} \approx \begin{cases} -n^2/8 - 2\varepsilon/\pi, & \text{for } n = 2, 4, 6, \dots, \\ -\varepsilon/\pi, & \text{for } n = 0, \end{cases} \quad (13)$$

as well as in the limit of very strong barriers,  $\varepsilon \gg 1$ :

$$k_{\text{large } \varepsilon} \approx -\frac{1}{2}\left(\frac{n}{2} + 1\right)^2. \quad (14)$$

Obviously, in the case of  $\varepsilon = 0$  eigenvalues (13) coincide with those for the free-space ring,  $k = -n^2/8$ , cf. Eq. (8). On the other hand, in the limit of  $\varepsilon \rightarrow \infty$ , Eq. (14) demonstrates that the effect of very tall barriers amounts to the shift of the even quantum number,  $n \rightarrow n + 2$ .

Proceeding to the presentation of the numerical solutions of the eigenstate problem, Fig. 1(a) shows examples of GS ( $n = 0$ ) and ES ( $n = 1$  and  $3$  for the odd ones, and  $n = 2$  for the even ES) wavefunctions produced by a numerical solution of Eq. (5) with  $\varepsilon = 0.5$ . The numerically found results for  $\varepsilon = 0.5$  are further summarized in Fig. 1(b), which displays the corresponding spectrum, i.e., the relation between eigenvalue  $k$  and quantum number  $n$ . The exact analytical expression (8) and the approximate one given by the top line in Eq. (13) are plotted, severally, by the bottom and top dashed curves in Fig. 1(b). In particular, the numerical value of the GS eigenvalue is  $k_{n=0}(\varepsilon = 0.5) \approx -0.1254$ , while approximation (13) yields  $(k_{\text{small } \varepsilon})_{n=0}(\varepsilon = 0.5) = -\varepsilon/\pi \approx -0.1591$  for the same case (note that Eq. (13) was derived for small  $\varepsilon$ , while  $\varepsilon = 0.5$  is not quite small).

For larger and very large values of  $\varepsilon$ , the numerically found eigenvalues and their comparison with the analytical approximations given by Eqs. (13) and (14) are presented in Figs. 2(a) and (b), for  $n = 0, 2, 4, 6$  and  $n = 0, 2$ , respectively. In particular, Figs. 2(b) demonstrates slow convergence to the asymptotic values (14) with the growth of  $\varepsilon$ .

### III. SPONTANEOUS SYMMETRY BREAKING (SSB) IN THE CASE OF SELF-FOCUSING ( $\sigma = +1$ )

#### A. An example: a particular exact solution

An exact solution of Eq. (4) with  $\sigma = +1$ , which demonstrates strongly broken symmetry, can be sought for as a “curtailed” bright soliton in the half-ring,  $-\pi/2 < x < +\pi/2$ :

$$U_{\text{sol}}(x) = \sqrt{2k} \text{sech}\left(\sqrt{2k}x\right), \quad (15)$$

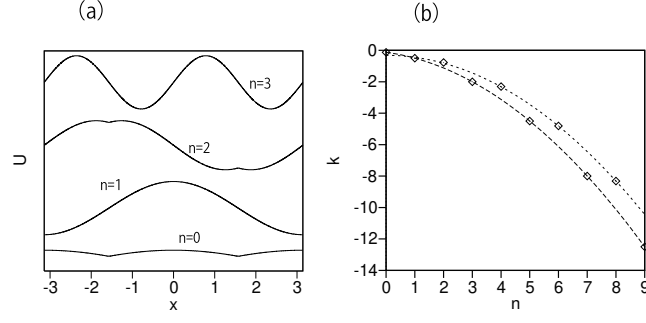


FIG. 1. (a) The GS ( $n = 0$ ) and ES ( $n = 1, 2, 3$ ) wavefunctions produced by numerical solution of Eq. (5) with  $\epsilon = 0.5$ . (b) Chains of rhombuses represent numerically found eigenvalues  $k$  vs. quantum number  $n$  for  $\epsilon = 0.5$ . The bottom and top dashed lines represent, respectively, the exact analytical expression (8) for the odd ESs and the analytical approximation (13) for the even ones (the difference between the corrections  $-2\epsilon/\pi$  and  $-\epsilon/\pi$  in the top and bottom lines of Eq. (13) is not clearly visible on the scale of the figure).

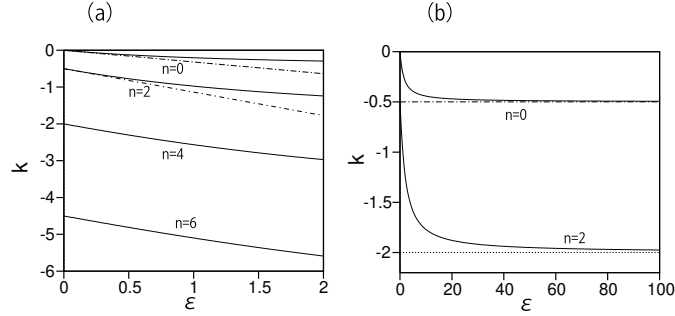


FIG. 2. (a) Eigenvalues  $k$  for even  $n$  vs. moderate values of the potential-barrier height,  $\epsilon$ , obtained from the numerical solution of Eq. (5). The dashed lines represent the approximation produced by Eq. (13). (b)  $k$  vs.  $\epsilon$  for  $n = 0$  and  $2$  for large values of  $\epsilon$ . The horizontal lines represent the respective asymptotic values (14).

and a constant solution in the other half-ring,  $-\pi < x < -\pi/2$  and  $+\pi/2 < x < +\pi$ :

$$U_{\text{const}} \equiv \sqrt{k}. \quad (16)$$

The conditions of the continuity at  $x = \pm\pi/2$ , i.e.,  $U_{\text{sol}}(x = \pm\pi/2) = U_{\text{const}} \equiv \sqrt{k}$ , along with the jump conditions (6) demonstrate, after a simple algebra, that such an exact solution exists at a single value of  $\epsilon$ , and at single value of  $k$ :

$$\epsilon = \frac{1}{\sqrt{2}\pi} \ln(\sqrt{2} + 1) \approx 0.198, \quad k = 4\epsilon^2 \approx 0.157. \quad (17)$$

It is relevant to calculate the norms of the two parts of the exact solution:

$$N_{\text{sol}} = \frac{2\sqrt{2}}{\pi} \ln(\sqrt{2} + 1) \approx 0.793, \quad (18)$$

$$N_{\text{const}} = \frac{2}{\pi} \ln^2(\sqrt{2} + 1) \approx 0.495, \quad (19)$$

with the ratio between them  $N_{\text{sol}}/N_{\text{const}} = \sqrt{2}/\ln(\sqrt{2} + 1) \approx 1.602$ . This stationary solution is plotted in Fig. 3. Direct simulations of Eq. (1) for the perturbed propagation of this stationary state demonstrate that it is *stable* (not shown here in detail).

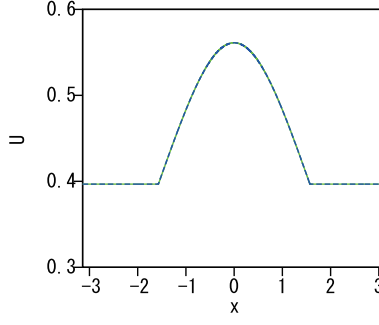


FIG. 3. The stable exact solution, given by expressions (15) and (16), with parameters taken as per Eq. (17), which demonstrates strong dissimilarity between the two half-circles. The dashed blue and solid green lines represent the analytical solution per se, and its counterpart produced by the numerical solution of Eq. (4), with the delta-functions replaced by the Gaussian approximation.

## B. The variational approximation (VA)

### 1. VA for stationary states: the prediction of SSB

Solutions of the full stationary nonlinear equation (4) are characterized by their total norm and energy:

$$N = N_1 = \int_{-\pi/2}^{+\pi/2} U^2(x) dx + \left( \int_{-\pi}^{-\pi/2} + \int_{+\pi/2}^{+\pi} \right) U^2(x) dx \equiv N_1 + N_2, \quad (20)$$

$$E = \int_{-\pi}^{+\pi} \left[ \frac{1}{2} \left( \frac{dU}{dx} \right)^2 - \frac{\sigma}{2} U^4 \right] dx + \epsilon \left[ U^2 \left( x = +\frac{\pi}{2} \right) + U^2 \left( x = -\frac{\pi}{2} \right) \right]. \quad (21)$$

To seek for stationary states of the nonlinear system, we first, apply VA, based on the following ansatz:

$$U(x) = \begin{cases} a_0 + a_1 \cos x, & \text{for } |x| < \pi/2, \\ a_0 - a_2 \cos x, & \text{for } \pi/2 < |x| < \pi. \end{cases} \quad (22)$$

The substitution of the ansatz in the jump conditions (6) leads to a relation between the amplitudes,

$$a_1 + a_2 = 2\epsilon a_0. \quad (23)$$

Further, the ansatz gives rise to the following expressions for norms  $N_1$  and  $N_2$  of the two layers, defined as per Eq. (20)

$$\begin{aligned} N_1 &= \pi a_0^2 + \pi a_1^2/2 + 4a_0 a_1, \\ N_2 &= \pi a_0^2 + \pi a_2^2/2 + 4a_0 a_2. \end{aligned} \quad (24)$$

The energy (21) corresponding to ansatz (22) is calculated analytically as

$$\begin{aligned} E &= \frac{\pi}{4} (a_1^2 + a_2^2) - \pi \left[ a_0^4 + \frac{3}{2} a_0^2 (a_1^2 + a_2^2) + \frac{3}{16} (a_1^4 + a_2^4) \right] \\ &\quad - 4a_0^3 (a_1 + a_2) - \frac{8}{3} a_0 (a_1^3 + a_2^3) + 2\epsilon a_0^2. \end{aligned} \quad (25)$$

In terms of ansatz (22), the symmetric state corresponds to  $a_1 = a_2$ . In view of the relation (23) between the amplitudes of the ansatz, SSB may be sought for by setting

$$a_1 = \epsilon a_0 + B/2, \quad a_2 = \epsilon a_0 - B/2, \quad (26)$$

the onset of SSB implying a transition to a solution with  $B \neq 0$ . In terms of amplitudes  $a_0$  and  $B$ , energy (25)  $E$  is rewritten as

$$E = \frac{\pi}{8}B^2 - \frac{3}{128}\pi B^4 + \left(\frac{\pi}{2}\epsilon^2 + 2\epsilon\right)a_0^2 - \left[\pi\left(1 + 3\epsilon^2 + \frac{3}{8}\epsilon^4\right) + 8\epsilon + \frac{16}{3}\epsilon^2\right]a_0^4 - \left[\pi\left(\frac{3}{4} + \frac{9}{16}\epsilon^2\right) + 4\epsilon\right]a_0^2B^2. \quad (27)$$

By the substitution of expressions (26) in the definition of the norm, based on Eqs. (20) and (24), one can express the basic amplitude  $a_0$  in terms of the total norm,  $N$ , and SSB amplitude  $B$ :

$$a_0^2 = \frac{N - \pi B^2/4}{2\pi + 8\epsilon + \pi\epsilon^2}. \quad (28)$$

Lastly, with the use of this relation, energy (27) is cast in the form of a cumbersome but tractable expression, written in terms of  $B$  and  $N$ :

$$E = c_0 + (c_{20} - c_{21}N)B^2 + c_4B^4, \quad (29)$$

where

$$c_0 = \frac{(\pi\epsilon^2/2 + 2\epsilon)N}{2\pi + 8\epsilon + \pi\epsilon^2} - \frac{[\pi(1 + 3\epsilon^2 + 3\epsilon^4/8) + 8\epsilon + 16\epsilon^3/3]N^2}{(2\pi + 8\epsilon + \pi\epsilon^2)^2}, \quad (30)$$

$$c_{20} = \frac{\pi^3/2 + 3\pi^2\epsilon + (\pi^3/4 + 4\pi)\epsilon^2 + \pi^2\epsilon^3/2}{(2\pi + 8\epsilon + \pi\epsilon^2)^2}, \quad (31)$$

$$c_{21} = \frac{\pi^2 + 10\pi\epsilon + (32 + 3\pi^2/8)\epsilon^2 + 35\pi\epsilon^3/6 + 3\pi^2\epsilon^4/8}{(2\pi + 8\epsilon + \pi\epsilon^2)^2}, \quad (32)$$

$$c_4 = \frac{7\pi^3/32 + 9\pi^2\epsilon/4 + (13\pi/2 + 3\pi^3/16)\epsilon^2 + 17\pi^2\epsilon^3/12 + 3\pi^3\epsilon^4/32}{(2\pi + 8\epsilon + \pi\epsilon^2)^2}. \quad (33)$$

The variational principle states that, for a given norm and fixed  $\epsilon$ , the system's GS is predicted as one with a positive value of  $B^2$  which provides for a minimum of energy (29), i.e.,

$$B^2 = \frac{c_{21}N - c_{20}}{2c_4}. \quad (34)$$

Because coefficients  $c_{20}$ ,  $c_{21}$ , and  $c_4$  are defined by expressions (31), (32), and (33) as positive ones, Eq. (34) predicts that SSB commences when the norm exceeds a critical value,

$$N_c(\epsilon) = c_{20}/c_{21}. \quad (35)$$

Further, general properties of the energy (Hamiltonian) imply that the eigenvalue corresponding to the present solution can be calculated as  $k = -\partial E/\partial N$ . The respective VA-produced result for the symmetric state, with  $B = 0$  in Eq. (26), is

$$k = k_s \equiv -\frac{\partial c_0}{\partial N} = -\frac{(\pi\epsilon^2/2 + 2\epsilon)}{2\pi + 8\epsilon + \pi\epsilon^2} + 2N \frac{[\pi(1 + 3\epsilon^2 + 3\epsilon^4/8) + 8\epsilon + 16\epsilon^3/3]}{(2\pi + 8\epsilon + \pi\epsilon^2)^2}. \quad (36)$$

while for the broken-symmetry state it is

$$k = k_{as} = k_s + \frac{(c_{21}N - c_{20})c_{21}}{(2c_4)}. \quad (37)$$

## 2. VA for nonstationary states: the stability analysis

The VA may also be applied as an approximation predicting the evolution of nonstationary ( $z$ -dependent) states (in particular, the onset of MI) [79, 80]. To this end, we use the Lagrangian of the full equation (1), in its nonstationary form:

$$L = \frac{1}{2} \int_{-\pi}^{+\pi} \left[ i \left( \frac{\partial u}{\partial z} u^* - \frac{\partial u^*}{\partial z} u \right) - \left| \frac{\partial u}{\partial x} \right|^2 + |u|^4 \right] dx - \epsilon \left[ \left| u \left( x = +\frac{\pi}{2} \right) \right|^2 + \left| u \left( x = -\frac{\pi}{2} \right) \right|^2 \right]. \quad (38)$$

To derive the dynamical version of the VA, we adopt the following *ansätze* for the symmetric and asymmetric states:

$$u_s^{(\text{VA})}(x, z) = a_0 [1 + \epsilon |\cos x|] \exp(ikz), \quad (39)$$

$$u_{\text{as}}^{(\text{VA})}(x, z) = [a_0 + \epsilon a_0 |\cos x| + b(z) \cos x] \exp(ikt), \quad (40)$$

where  $a_0$  and  $k$  are real constants, while  $b(z)$  is a complex variable amplitude which accounts for the onset of *spatial modulation* of the symmetric state, or, in other words, for the initiation of SSB. Note that the norm (20) corresponding to the symmetric ansatz (39) is

$$N_s = a_0^2 (2\pi + 8\epsilon + \pi\epsilon^2). \quad (41)$$

Naturally, the expression for  $U(x) \equiv |u_s^{(\text{VA})}(x, z)|$ , as given by Eq. (39), is identical to ansatz (22) adopted above for stationary solutions, in the case of the symmetric state, as it follows from Eq. (26) with  $B = 0$ .

The substitution of ansatz (40) in Lagrangian (38) yield the corresponding VA Lagrangian,

$$L_{\text{VA}} = i \frac{\pi}{2} \left( \frac{db}{dz} b^* - \frac{db^*}{dz} b \right) - \pi k |b|^2 - \frac{\pi}{2} |b|^2 + \left[ \frac{1}{2} a_0^2 ((b^*)^2 + b^2) + 2a_0^2 |b|^2 \right] \left( \pi + \frac{16}{3}\epsilon + \frac{3}{4}\pi\epsilon^2 \right) + \frac{3}{8}\pi |b|^4, \quad (42)$$

with  $*$  standing for the complex conjugate. Then, the evolution equation for  $b(z)$  is derived from the VA Lagrangian (42) as the corresponding Euler-Lagrange (EL) equation, *viz.*,

$$i \frac{db}{dz} = \left( k + \frac{1}{2} \right) b - \left( 1 + \frac{16}{3\pi}\epsilon + \frac{3}{4}\epsilon^2 \right) a_0^2 (b^* + 2b) - \frac{3}{4} |b|^2 b. \quad (43)$$

The onset of the instability is signaled by the emergence of an exponentially growing solution of the linearized version of Eq. (43) for  $b(z)$ . To analyze this scenario, the linearized equation is split in real and imaginary parts, by substituting  $b(z) \equiv b_1(z) + ib_2(z)$ :

$$\frac{db_1}{dz} = \left[ \left( k + \frac{1}{2} \right) - a_0^2 \left( 1 + \frac{16}{3\pi}\epsilon + \frac{3}{4}\epsilon^2 \right) \right] b_2, \quad (44)$$

$$-\frac{db_2}{dz} = \left[ \left( k + \frac{1}{2} \right) - 3a_0^2 \left( 1 + \frac{16}{3\pi}\epsilon + \frac{3}{4}\epsilon^2 \right) \right] b_1. \quad (45)$$

Solutions to this system of linear equations are looked for as  $b_{1,2}(z) = b_{1,2}^{(0)} \exp(\lambda z)$ . A straightforward calculation yields the value of the instability growth rate  $\lambda$ , as

$$\lambda^2 = \pi \left[ \left( k + \frac{1}{2} \right) - a_0^2 \left( 1 + \frac{16}{3\pi}\epsilon + \frac{3}{4}\epsilon^2 \right) \right] \times \left[ 3a_0^2 \left( 1 + \frac{16}{3\pi}\epsilon + \frac{3}{4}\epsilon^2 \right) - \left( k + \frac{1}{2} \right) \right]. \quad (46)$$

In the framework of the present approximation, MI takes place if Eq. (46) yields  $\lambda^2 > 0$ . As it follows from Eq. (46) and expressions (36) and (41) for the propagation constant and norm of the symmetric state, this condition eventually amounts to

$$N > N_c = \frac{\pi [2\pi^2 + 12\pi\epsilon + (\pi^2 + 16)\epsilon^2 + 2\epsilon^3]}{4\pi^2 + 40\pi\epsilon + (3\pi^2/2 + 128)\epsilon^2 + 70\pi\epsilon^3/3 + 3\pi^2\epsilon^4/2}. \quad (47)$$

Note that the critical value of the norm, given by Eq. (47), is *identical* to one for the onset of SSB, which was found above in the form of Eqs. (35) and (31), (32), hence the MI is precisely the instability mode of the symmetric state which determines the commencement of the SSB.

The comparison of the VA predictions with numerical results is provided below in Figs. 4, 5, and 7(a).

### C. The analytical approximation for large $\epsilon$

Another approximation can be elaborated in the limit of large  $\epsilon$ , when the ring is split by the delta-functional barriers in two half-rings, which are nearly isolated from each other. The weak residual coupling between the two half-rings implies that weak self-focusing nonlinearity, measured by the squared amplitude of the solution,  $U_0^2$  (see Eqs. (9)), is sufficient to break the symmetry. This means that, in the zero-order approximation, in the half-ring  $-\pi/2 < x < +\pi/2$  one may take the obvious solutions of the linearized equation (5),

$$U(x) = U_0 \cos(\sqrt{-2k}x). \quad (48)$$

The first nonlinear correction to this solution follows from the elementary formula

$$\cos^3(\sqrt{-2k}x) = (3/4) \cos(\sqrt{-2k}x) + (1/4) \cos(3\sqrt{-2k}x). \quad (49)$$

The former term on the right-hand side of Eq. (49) implies that  $k$  in Eq. (4) with  $\sigma = +1$  is replaced by the corrected value,

$$k \rightarrow k - (3/4)U_0^2, \quad (50)$$

and the third-harmonic correction added to the fundamental one (48) is

$$U_3(x) = -(32k)^{-1}U_0^3 \cos(3\sqrt{-2k}x), \quad (51)$$

In the limit of  $\epsilon = \infty$ , the boundary conditions for GS (48), become  $U(x = \pm\pi/2) = 0$ , implying  $k = -1/2$ . At large but finite  $\epsilon$ , a small correction is introduced:

$$k = -1/2 + \delta k, \text{ i.e., } \sqrt{-2k} \approx 1 - \delta k. \quad (52)$$

On the other hand, the contribution of correction (51) to the boundary conditions (6) is negligible in the first approximation because  $\cos(3x) = 0$  at  $x = \pm\pi/2$ . The only essential correction originating from the weak nonlinearity is produced by the shift (50) of the propagation constant, which replaces  $U_0 \cos(\sqrt{-2k}x)$  in Eq. (48) by

$$U(x) \approx U_0 \cos((1 - \delta k + (3/4)U_0^2)x), \quad (53)$$

where expression (52) is substituted for  $\sqrt{-2k}$ .

The GS solution with broken symmetry is approximated by expressions (53) in the two half-rings, with different amplitudes,  $U_0 \rightarrow U_{1,2}$ . The substitution of these expressions in the condition of the continuity of  $U(x)$  at  $x = \pm\pi/2$  yields the following equation, in the lowest approximation with respect to small parameters  $\delta k$  and  $U_{1,2}^2$ :

$$U_1 [\delta k - (3/4)U_1^2] = U_2 [\delta k - (3/4)U_2^2] \quad (54)$$

Further, the substitution of expressions (53) with amplitudes  $U_{1,2}$  in the jump condition (6) leads to the following equation, which is also written in the lowest approximation with respect to small parameters  $\delta k$ ,  $U_{1,2}^2$ , and  $1/\epsilon$ :

$$\frac{2}{\pi\epsilon} (U_1 + U_2) = \delta k \cdot (U_1 + U_2) - (3/4) (U_1^3 + U_2^3). \quad (55)$$

When writing Eq. (55), the right-hand side in Eq. (6) is taken in the symmetrized form, as the half-sum of  $U(x = \pm\pi/2)$  corresponding to the two half-rings (because of the continuity condition, the half-sum is the same as  $U(x = \pm\pi/2)$  corresponding to either half-ring, the use of the symmetrized form making it easier to solve the equations).

For the symmetry-breaking GS, with  $U_1 \neq U_2$ , one can cancel factor  $(U_1 - U_2)$  in the continuity equation (54), and cancel factor  $(U_1 + U_2)$  in the jump equation (55), arriving at the following equations:

$$U_1^2 + U_2^2 + U_1 U_2 = (4/3)\delta k, \quad (56)$$

$$U_1^2 + U_2^2 - U_1 U_2 = (4/3) [\delta k - 2/(\pi\epsilon)]. \quad (57)$$

The combination of Eqs. (56) and (57) give rise to a simple relation,

$$U_1 U_2 = 4/(3\pi\epsilon). \quad (58)$$

Using it to eliminate  $U_2$  in favor of  $U_1$ , one arrives at the biquadratic equation for  $U_1$ :

$$U_1^4 - \frac{4}{3} \left( \delta k - \frac{1}{\pi\epsilon} \right) U_1^2 + \left( \frac{4}{3\pi\epsilon} \right)^2 = 0. \quad (59)$$

The result following from Eq. (59) is that the symmetry-breaking GS state exists under the following threshold condition,

$$\delta k > (\delta k)_{\text{thr}} \equiv 3/(\pi\epsilon). \quad (60)$$

The amplitude at the threshold point is found by substituting  $U_1 = U_2 \equiv U_{\text{thr}}$  in Eq. (58), which yields  $U_{\text{thr}}^2 = 4/(3\pi\epsilon)$ . The respective critical value of the norm, which determines the onset of SSB at large  $\epsilon$ , is

$$N_c = \pi U_{\text{thr}}^2 \equiv 4/(3\epsilon) \quad (61)$$

(cf. the prediction (47) provided by the VA). As shown below in Fig. 5, this approximation is accurate enough at very large values of  $\epsilon$ .

#### D. Numerical findings

Stationary solutions of Eq. (1) with  $\sigma = +1$  were produced by means of the well-known [81] imaginary-time-evolution method. A typical example of a numerically found stable stationary mode  $U(x)$  with the broken symmetry, i.e., a result of SSB, is plotted in Fig. 4(a) for  $\epsilon = 0.5$  and  $N = 1.02$ . The corresponding variational ansatz (22) with the VA-produced coefficients, *viz.*,

$$a_0 = 0.3004, a_1 = 0.2406, a_2 = 0.0571, \quad (62)$$

is plotted by the dashed lines.

As a measure of the symmetry breaking, we define

$$R = (N_1 - N_2)/(N_1 + N_2), \quad (63)$$

with  $N_{1,2}$  defined in Eq. (20). Figure 4(b) summarizes the numerical results obtained for  $\epsilon = 0.5$ , in the form of the bifurcation diagram represented by the dependence  $R(N)$  (the chain of rhombuses), while the dashed line represents the VA prediction for the same case, as produced by Eqs. (24), (26), and (34). It is seen that the SSB bifurcation is of the forward (supercritical [74]) type. Another SSB characteristic, *viz.*, dependences  $k(N)$  for the symmetric and asymmetric states, and their comparison to the VA prediction, produced by Eqs. (36) and (37), is shown in Fig. 4(c).

The results are further summarized in Fig. 5, which reports numerically found values of the critical norm at the SSB point,  $N_c$ , for  $\epsilon = 0.1, 0.5, 1.5$ , and  $3$ , along with the curve plotting the VA prediction (47) for the  $N_c(\epsilon)$  dependence. Note that the value  $N_c(\epsilon = 0) = \pi/2$  corresponds to the commonly known threshold of MI (alias the Benjamin-Feir instability [82, 83]) for the uniform (CW) state in the ring [63]. Figures 4 and 5 demonstrate high accuracy of the VA, in comparison to the numerical findings. As mentioned above, the decrease of  $N_c$  with the increase of  $\epsilon$  is a natural property of the system, as larger  $\epsilon$  means weaker coupling between two semi-rings, hence weaker nonlinearity is sufficient to initiate SSB.

The stability of the symmetric and asymmetric stationary states was verified by direct simulations of their perturbed evolution in the framework of Eq. (1). An example is presented in Fig. 6 for  $\epsilon = 0.5$  and  $N = 1.02$ . Figure 6(a) shows the corresponding evolution of the asymmetry parameter  $R$ , defined as per Eq. (63). It is seen that  $R$  remains practically constant for the stable asymmetric state. On the other hand, the instability of the symmetric one leads to large oscillations of  $R$  between 0 and 0.435, i.e., periodic oscillations between symmetric and strongly asymmetric configurations. The oscillations are illustrated in Fig. 6(b) by means of 7 snapshots of  $|u(x)|$ , starting from the initial symmetric configuration at  $z = 0$  and periodically attaining a fully asymmetric one (e.g., at  $z = 250$ ).

While the above examples, presented in Figs. 4 and 6, display the numerical and VA-predicted analytical results for the system with relatively weak potential barriers ( $\epsilon = 0.5$  in Eq. (1)), the findings obtained for much stronger barriers, with  $\epsilon = 3$ , are presented in Fig. 7. In particular, Fig. 7(a) demonstrates that the VA provides a sufficiently accurate approximation for the SSB diagram (the  $R(N)$  curve) in this case too.

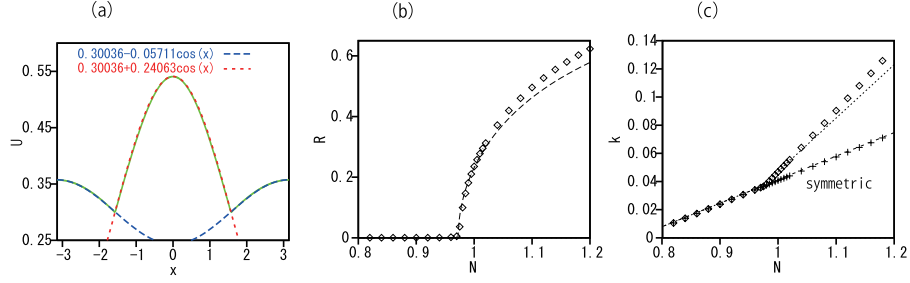


FIG. 4. (a) The solid green lines represent the numerically obtained profile of the stable asymmetric mode  $U(x)$  with  $\sigma = +1$  (self-focusing nonlinearity),  $\epsilon = 0.5$  and  $N = 1.02$ . The corresponding ansatz (22) with coefficients (62) predicted by the VA (and printed in the panel), is plotted by the dashed blue and red lines. (b) The numerically found value of asymmetry measure (63) vs. the total norm,  $N$ , at  $\epsilon = 0.5$ . The dashed line is the VA prediction for  $R$ , see Eqs. (24), (26), and (34). (c) Numerically obtained values of the propagation constant  $k$  for the symmetric (pluses) and symmetry-breaking (rhombuses) modes vs.  $N$ . The dashed lines represent the respective VA prediction, see Eqs. (36) and (37).

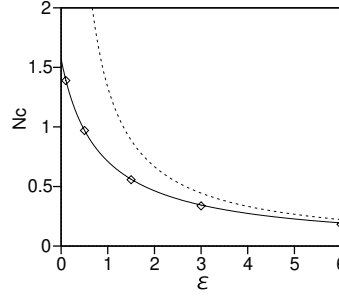


FIG. 5. The continuous curve shows the critical value  $N_c$  at the SSB point in the model with self-focusing ( $\sigma = +1$ ), as predicted by the VA, see Eq. (47). The prediction of the approximation for large  $\epsilon$ , produced by Eq. (61), is plotted by the dashed curve. Rhombuses represent numerically found values of  $N_c$ .

#### IV. SPONTANEOUS ANTISYMMETRY BREAKING (SASB) IN THE CASE OF SELF-DEFOCUSING ( $\sigma = -1$ )

##### A. The variational approximation (VA)

###### 1. VA for stationary antisymmetric states

As mentioned above, in the case of the self-repulsive nonlinearity, which corresponds to  $\sigma = -1$  in Eq. (1), one cannot expect a transition of the GS into a symmetry-breaking shape, but destabilization of the spatially odd (antisymmetric) lowest ES is possible [50, 51]. In the framework of VA, a solution of Eq. (1), with  $\sigma = -1$ , for the lowest ES may be approximated by the ansatz which is antisymmetric with respect to points  $x = \pm\pi/2$ , where the delta-functional barriers are set:

$$u_{\text{anti}}^{(\text{VA})}(x) = [A_1 \cos x + A_3 \cos(3x)] \exp(ikz). \quad (64)$$

cf. ansatz (39) for the spatially even GS. The norm of this ansatz is

$$N_{\text{anti}} = \pi (A_1^2 + A_3^2), \quad (65)$$

The substitution of the ansatz in Lagrangian (38) (with the opposite sign in front of  $|u|^4$ , which corresponds to  $\sigma = -1$ ), readily produces the effective VA Lagrangian,

$$(L_{\text{VA}})_{\text{anti}} = -\pi(A_1^2 + A_3^2)k - \frac{\pi}{2}(A_1^2 + 9A_3^2) - \frac{3\pi}{8}(A_1^4 + A_3^4 + 4A_1^2A_3^2) + \frac{\pi}{2}A_1^3A_3. \quad (66)$$

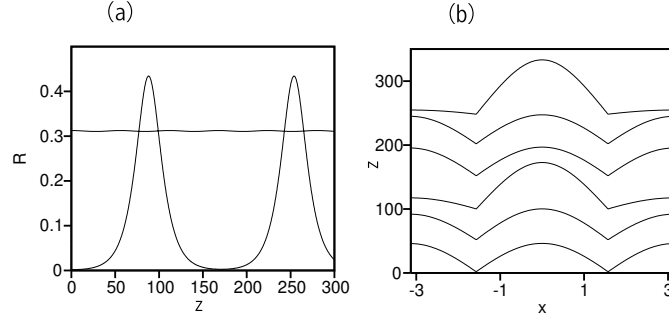


FIG. 6. (a) The evolution of the asymmetry measure  $R(z)$  (see Eq. (63)) for the unstable symmetric and stable asymmetric states in the model with the self-focusing nonlinearity ( $\sigma = +1$ ), which coexist at  $\epsilon = 0.5$  and  $N = 1.02$ . (b) Seven snapshots of  $|u(x)|$  at  $z = 50n$  ( $n = 0, 1, 2, \dots, 6$ ), starting from the symmetric solution with a very small perturbation added to it.

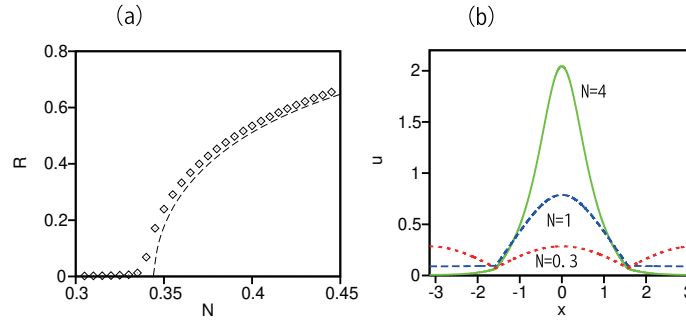


FIG. 7. (a) The chain of rhombuses presents the dependence of the asymmetry measure (63) on the total norm,  $N$ , as produced by the numerical solution of Eq. (4) with  $\sigma = +1$  (self-focusing) and  $\epsilon = 3$ . The dashed line shows the same dependence, as predicted by the VA, see Eq. (47). (b) Numerically found profiles of  $U(x)$ , with  $\epsilon = 3$ , for a stable symmetric mode with  $N = 0.3$  (the red dotted line), and stable asymmetric ones, with  $N = 1$  and  $4$  (the blue dashed and green solid lines, respectively).

Note that this expression does not include parameter  $\epsilon$ , as ansatz (64) vanishes at the points where the delta-functional barriers are set. Then, parameters of the VA-approximated odd mode are determined by the EL equations,  $\partial(L_{\text{VA}})_{\text{anti}}/\partial(A_{1,3}) = 0$ . Figure 8(a) displays an example of the stationary state, as produced by the numerical solution of Eq. (4) for  $N = 2.5$ , along with its VA-predicted counterpart, with amplitudes  $A_1 = 0.8912$  and  $A_3 = -0.00383$ , as given by the EL equations. Figure 8(b) represents the family of the lowest-ES stationary solutions by means of the respective  $k(N)$  dependence, as obtained from the numerical results (the chain of rhombuses), and as predicted by the VA, including its simplified version with  $A_3 = 0$  in ansatz (64), the latter one amounting to  $k = -1/2 - 3N/(4\pi)$ .

## 2. Nonstationary VA: the stability analysis of the antisymmetric state

Similar to the VA for the nonstationary states with broken symmetry, which was developed in the previous section, we here address the dynamics of states breaking the antisymmetry. For this purpose, the following ansatz is adopted, with the complex amplitude  $b(z)$  of the SASB perturbation (cf. Eq. (40)):

$$u_{\text{SASB}}^{(\text{VA})}(x, z) = [A_1 \cos x + A_3 \cos(3x) + b(z)(1 + \epsilon |\cos x|)] e^{ikz}. \quad (67)$$

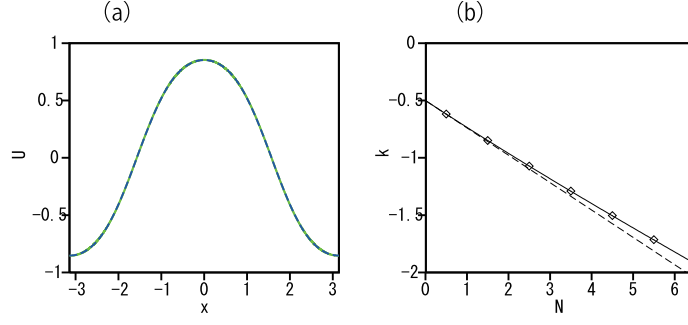


FIG. 8. (a) The profile of the stable lowest excited state (ES), found as the numerical solution of Eq. (4) with  $\sigma = -1$ ,  $\epsilon = 2$ , and the total norm  $N = 2.5$ , is plotted by the solid green line. The profile is antisymmetric (odd) with respect to points  $x = \pm\pi/2$ , where the delta-functional potential barriers are set. The dashed blue line (which actually completely overlaps with the solid green one) represents the VA-predicted counterpart of this state, given by ansatz (64), with coefficients  $A_1 = 0.8912$  and  $A_3 = -0.0383$ . (b) The  $k(N)$  dependence for the lowest-ES solution, as predicted by the VA based on ansatz (64) (the solid line), and its simplified version with  $A_3 = 0$  (the dashed line). The chain of rhombuses shows values of  $k(N)$  obtained from the numerical solution.

The substitution of this ansatz in the Lagrangian and neglecting terms which are quartic with respect to the perturbation amplitude, we obtain

$$\begin{aligned}
 (L_{\text{VA}})_{\text{SASB}} = & i \left( \pi + 4\epsilon + \frac{\pi}{2}\epsilon^2 \right) \left( \frac{\partial b}{\partial z} b^* - \frac{\partial b^*}{\partial z} b \right) \\
 & - (2\pi + 8\epsilon + \pi\epsilon^2) k |b|^2 - \left( 2\epsilon + \frac{\pi}{2}\epsilon^2 \right) |b|^2 \\
 & - \frac{A_1^2}{2} \left( \pi + \frac{16}{3}\epsilon + \frac{3\pi}{4}\epsilon^2 \right) (b^2 + b^{*2} + 4|b|^2) \\
 & - \frac{A_3^2}{2} \left( \pi + \frac{144}{35}\epsilon + \frac{\pi}{2}\epsilon^2 \right) (b^2 + b^{*2} + 4|b|^2) \\
 & - A_1 A_3 \left( \frac{16}{15}\epsilon + \frac{\pi}{4}\epsilon^2 \right) (b^2 + (b^*)^2 + 4|b|^2).
 \end{aligned} \tag{68}$$

Further, following the pattern of the analysis developed in the previous section, we derive the linear EL equation for  $b(z)$  from Lagrangian (68), split it in the real and imaginary parts by substituting  $b(z) = b_1(z) + ib_2(z)$ , and look for solutions with  $b_{1,2}(z) \sim \exp(\lambda z)$ , cf. Eqs. (43)-(46). Skipping technical details, the VA predicts the onset of instability of the antisymmetric state, accounted for by the emergence of  $\lambda^2 > 0$ , when norm  $N$  of the stationary antisymmetric solutions exceeds the respective critical value,  $N_{\text{ce}}$ . In particular, this value takes a simple form if one uses the simplified ansatz (67) with  $A_3 = 0$ , when the parameters of the antisymmetric state are  $A_1^2 = N/\pi$  and  $k = -1/2 - 3N/(4\pi)$ :

$$N_{\text{ce}} = \frac{2\pi^2 + 4\pi\epsilon}{3\pi + 20\epsilon + 3\pi\epsilon^2}. \tag{69}$$

This prediction is compared to numerical results below in Fig. 10.

## B. Numerical findings

An example of the instability of the lowest ES (antisymmetric mode) is demonstrated in Fig. 9(a) with the help of direct simulations of Eq. (1) with  $\sigma = -1$  and  $\epsilon = 0.5$ , for two cases, with total norms  $N = 1.65$  and  $1.80$ . Similar to Fig. 6(a), the oscillatory regime initiated by the instability is plotted by means of the respective dependences of the asymmetry measure (63) on  $z$  (note that  $R = 0$  for symmetric and antisymmetric states alike). Figure 9(b) illustrates the shape of the oscillatory state by means of snapshots of  $\text{Re}(u(x, t))$  and  $\text{Im}(u(x, t))$  for  $N = 1.80$  at  $z = 50$ , when the asymmetry measure takes a large value,  $R = 0.4853$ . The picture clearly demonstrates that the antisymmetry is indeed broken, as the zero points are shifted from  $x = \pm\pi/2 \approx \pm 1.571$  to  $x \approx \pm 1.815$ . Note that values of  $|u(x, z)|$

at points  $x = \pm\pi/2$  are nonzero but small in this configuration, therefore the corresponding jumps of  $\partial u/\partial x$  at these points are inconspicuous in Fig. 9(b).

For the parameters fixed in Figs. 9(a,b) ( $\sigma = -1$ ,  $\epsilon = 0.5$ ), the SASB transition is systematically displayed in Fig. 9(c) by dint of the dependence of the maximum (peak) value  $R_p$ , of the oscillating asymmetry parameter  $R$ , on  $N$ . The gradual increase of  $R_p$  with  $N$  demonstrates a continuous SASB transition, cf. Fig. 4(b) for the SSB transition in the self-focusing system. On the other hand, on the contrary to the usual situation with SSB, which occurs under the action of the self-focusing, Eqs. (1) and (4) do not produce any stationary state with broken antisymmetry at  $N > N_{ce}$  (above the SASB threshold). Thus, the conclusion is that the SASB transition leads to the establishment of the robust oscillating states (breathers).

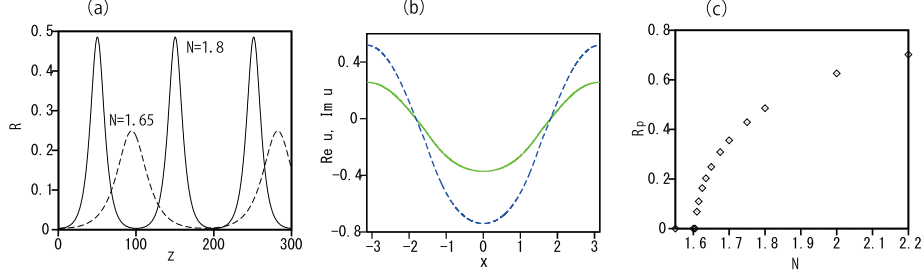


FIG. 9. (a) The evolution of the asymmetry measure (63) of the unstable antisymmetric (lowest-ES) modes, produced by simulations of Eq. (1) with  $\sigma = -1$  and  $\epsilon = 0.5$ , for two values of the total norm:  $N = 1.80$  and  $1.65$  (solid and dashed lines, respectively). (b)  $\text{Re}(u(x,t))$  and  $\text{Im}(u(x,t))$  (the solid green and dashed blue lines, respectively) at  $z = 50$  for  $N = 1.8$ . (c) The maximum (peak) value of the asymmetry measure,  $R_p$ , vs. the total norm,  $N$ , for the unstable antisymmetric states at  $\epsilon = 0.5$ .

Finally, the dependence of the critical norm  $N_{ce}$ , at which SASB commences, on  $\epsilon$  is plotted in Fig. 10. The chain of rhombuses represents numerically found values of  $N_{ce}$ , while the dashed curve corresponds to Eq. (69), which is predicted by the simplified VA, with  $A_3 = 0$  in ansatz (67) (the result of the full VA, including  $A_3 \neq 0$ , is presented too, being virtually the same). As well as the dependence  $N_c(\epsilon)$  for the SSB, which is plotted above in Fig. 5, the present one demonstrates the decrease of the critical norm with the increase of  $\epsilon$ , which is explained by the same reason: the weaker coupling between the half-ring boxes, in the case of larger  $\epsilon$ , allows weaker defocusing nonlinearity to initiate SASB. The discrepancy between the numerically found and VA-predicted values of  $N_{ce}$ , observed in Fig. 10, is explained by insufficient accuracy of ansatz (67).

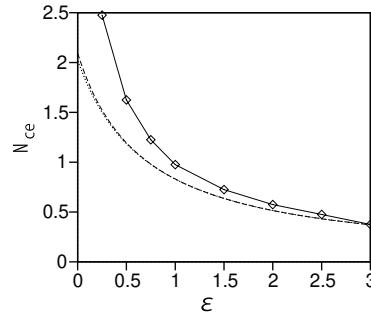


FIG. 10. Rhombuses represent the critical value  $N_{ce}$  for the onset of the antisymmetry-breaking instability as a function of  $\epsilon$ , obtained from the numerical solution of Eq. (1) with  $\sigma = -1$ . The nearly identical dashed and dotted lines represent the values of  $N_{ce}$  as predicted by VA with  $A_3 = 0$  and  $A_3 \neq 0$ , respectively, in ansatz (67).

## V. CONCLUSION

The objective of this work is to introduce a basic setting for the implementation of SSB (spontaneous symmetry breaking) and SASB (spontaneous antisymmetry breaking) under the action of the self-focusing and defocusing cubic

nonlinearity, respectively, in the ring split in two boxes by delta-functional potential barriers with strength  $\epsilon$ , set at diametrically opposite points. The setting can be implemented in optics and for matter waves in BEC. First, the spectrum of the linearized model was found in the approximate analytical and full numerical forms. In the framework of the nonlinear system, both SSB and SASB were predicted sufficiently accurately by the VA (variational approximation), and were studied systematically by means of numerical methods. In addition, a particular exact analytical solution with strong asymmetry was found, and the approximation for large  $\epsilon$  was presented. In the case of the self-focusing nonlinearity, the SSB-initiating instability of the spatially symmetric GS (ground state) is actually the MI (modulational instability) driven by the self-focusing. The SSB gives rise to the supercritical bifurcation, which creates stable stationary asymmetric states. In the case of the defocusing nonlinearity, the symmetric GS remains stable, while SASB destabilizes the lowest spatially antisymmetric ES (excited state), replacing it by a robust oscillatory mode with broken antisymmetry.

As an extension of the work, it may be interesting to introduce a similar two-component model, based on a pair of linearly or nonlinearly coupled NLS equations, cf. the two-component system in the potential box split by the central delta-functional barrier [84].

## ACKNOWLEDGMENTS

The work of B.A.M. was supported, in part, by the Israel Science Foundation through grant No. 1695/22.

## DATA AVAILABILITY

Details of numerical data can be provided on a reasonable request.

- 
- [1] *Spontaneous Symmetry Breaking, Self-Trapping, and Josephson Oscillations* (B.A. Malomed, Editor, Springer, Berlin, 2013).
  - [2] E. B. Davies, Symmetry breaking in a non-linear Schrödinger equation. *Commun. Math. Phys.* **64**, 191–210 (1979).
  - [3] J. C. Eilbeck, P. S. Lomdahl, and A. C. Scott, The discrete self-trapping equation. *Physica D* **16**, 318–338 (1985).
  - [4] E. M. Wright, G. I. Stegeman, and S. Wabnitz, Solitary-wave decay and symmetry-breaking instabilities in two-mode fibers, *Phys. Rev. A* **40**, 4455–4466 (1989).
  - [5] F. K. Abdullaev, R. M. Abrarov, and S. A. Darmanyan, Dynamics of solitons in coupled optical fibers. *Opt. Lett.* **14**, 131–133 (1989).
  - [6] C. Paré and M. Flórjańczyk, Approximate model of soliton dynamics in all-optical couplers, *Phys. Rev. A* **41**, 6287–6295 (1990).
  - [7] A. I. Maimistov, Propagation of a light pulse in nonlinear tunnel-coupled optical waveguides, *Kvant. Elektron.* **18**, 758–761 [*Sov. J. Quantum Electron.* **21**, 687–690 (1991)].
  - [8] A. W. Snyder, D. J. Mitchell, L. Poladian, D. R. Rowland, and Y. Chen, Physics of nonlinear fiber couplers, *J. Opt. Soc. Am. B* **8**, 2101–2118 (1991).
  - [9] N. Akhmediev and A. Ankiewicz, Novel soliton states and bifurcation phenomena in nonlinear fiber couplers, *Phys. Rev. Lett.* **70**, 2395–2398 (1993).
  - [10] J. M. Soto-Crespo and N. Akhmediev, Stability of the soliton states in a nonlinear fiber coupler. *Phys. Rev. E* **48**, 4710–4715 (1993).
  - [11] I. M. Uzunov, R. Muschall, M. Göllés, Y. S. Kivshar, B. A. Malomed, and F. Lederer, Pulse switching in nonlinear fiber directional couplers, *Phys. Rev. E* **51**, 2527–2537 (1995).
  - [12] K. S. Chiang, Intermodal dispersion in two-core optical fibers, *Opt. Lett.* **20**, 997–999 (1995).
  - [13] P. L. Chu, Yu. S. Kivshar, B. A. Malomed, G. D. Peng, and M. L. Quiroga-Teixeiro, Soliton controlling, switching, and splitting in fused nonlinear couplers, *J. Opt. Soc. Am. B* **12**, 898 (1995).
  - [14] B. A. Malomed, I. Skinner, P. L. Chu, and G. D. Peng, Symmetric and asymmetric solitons in twin-core nonlinear optical fibers, *Phys. Rev. E* **53**, 4084–4081 (1996).
  - [15] N. F. Smyth and A. L. Worthy, Dispersive radiation and nonlinear twin-core fibers, *J. Opt. Soc. Am. B* **14**, 2610–2617 (1997).
  - [16] A. Mostofi, B. A. Malomed, and P. L. Chu, Effect of coupling fluctuations on cw switching in nonlinear optical couplers. *Opt. Commun.* **137**, 244–248 (1997).
  - [17] V. H. Nguyen, L. X. T. Tai, I. Bugar, M. Longobucco, R. Buczynski, B. A. Malomed, and M. Trippenbach, Reversible ultrafast soliton switching in dual-core highly nonlinear optical fibers, *Opt. Lett.* **45**, 5221–5224 (2020).
  - [18] M. Romagnoli, S. Trillo, and S. Wabnitz, Soliton switching in nonlinear couplers. *Opt. Quantum Electron.* **24**, S1237–S1267 (1992).

- [19] B. A. Malomed, A variety of dynamical settings in dual-core nonlinear fibers, In: *Handbook of Optical Fibers*, Vol. 1, pp. 421-474 (G.-D. Peng, Editor: Springer, Singapore, 2019).
- [20] P. G. Kevrekidis, Z. Chen, B. A. Malomed, D. J. Frantzeskakis, and M. I. Weinstein, Spontaneous symmetry breaking in photonic lattices: theory and experiment, *Phys. Lett. A* **340**, 275–280 (2005).
- [21] M. Belić, D. Jović, S. Prvanović, D. Arsenović, and M. Petrović, Counterpropagating self-trapped beams in optical photonic lattices, *Opt. Exp.* **14**, 794-799 (2006).
- [22] G. Herring, P. G. Kevrekidis, B. A. Malomed, R. Carretero-Gonzalez, and D. J. Frantzeskakis, Symmetry breaking in linearly coupled dynamical lattices. *Phys. Rev. E* **76**, 066606 (2007).
- [23] P. P. Beličev, I. Ilić, M. Stepić, L. Hadžievski, C. B. Lou, S. Suntsov, C. E. Rüter, and D. Kip, Spontaneous symmetry breaking of gap solitons in defect-loaded uniform one-dimensional photonic lattices, *Phys. Rev. A* **88**, 23858 (2013).
- [24] V. Savona, Spontaneous symmetry breaking in a quadratically driven nonlinear photonic lattice, *Phys. Rev. A* **96**, 033826 (2017).
- [25] M. Liu, D. A. Powell, I. V. Shadrivov, M. Lapine, Y. S. Kivshar, Spontaneous chiral symmetry breaking in metamaterials. *Nature Commun.* **5**, 4441 (2014).
- [26] S. Campione, S. Liu, L. I. Basilio, L. K. Warne, W. L. Langston, T. S. Luk, J. R. Wendt, J. L. Reno, G. A. Keeler, I. Brener, and M. B. Sinclair, Broken Symmetry Dielectric Resonators for High Quality Factor Fano Metasurfaces, *ACS Photonics* **3**, 2362-2367 (2016).
- [27] T. Heil, I. Fischer, W. Elsässer, J. Mulet, and C. R. Mirasso, Chaos synchronization and spontaneous symmetry-breaking in symmetrically delay-coupled semiconductor lasers, *Phys. Rev. Lett.* **86**, 795–798 (2000).
- [28] P. Hamel, S. Haddadi, F. Raineri, P. Monnier, G. Beaudoin, I. Sagnes, A. Levenson, A. M. Yacomotti, Spontaneous mirror-symmetry breaking in coupled photonic-crystal nanolasers, *Nature Photonics* **9**, 311–315 (2015).
- [29] N. D. Fortman, R. Kolkowski, D. Pal, S. R. K. Rodriguez, P. Schall, and A. F. Koenderink, Spontaneous symmetry breaking in plasmon lattice lasers, *Science Advances* **10**, eadn2723 (2024).
- [30] H. Sakaguchi, Pattern formation in a system with spontaneously-broken rotational symmetry. *Prog. Theor. Phys.* **99**, 33-43 (1998).
- [31] A. Sigler and B. A. Malomed, Solitary pulses in linearly coupled cubic-quintic Ginzburg-Landau equations, *Physica D* **212**, 305–316 (2005).
- [32] Z. Lin, H. Ramezani, T. Eichelkraut, T. Kottos, H. Cao, and D. N. Christodoulides, Unidirectional Invisibility Induced by  $\mathcal{PT}$ -Symmetric Periodic Structures, *Phys. Rev. Lett.* **106**, 213901 (2011).
- [33] R. Driben and B. A. Malomed, Stability of solitons in parity-time-symmetric couplers, *Opt. Lett.* **36**, 4323-4325 (2011).
- [34] N. V. Alexeeva, I. V. Barashenkov, A. A. Sukhorukov, and Y. S. Kivshar, Optical solitons in  $\mathcal{PT}$ -symmetric nonlinear couplers with gain and loss, *Phys. Rev. A* **85**, 063837 (2012).
- [35] M. Li and T. Xu, Dark and antidark soliton interactions in the nonlocal nonlinear Schrödinger equation with the self-induced parity-time-symmetric potential, *Phys. Rev. E* **91**, 033202 (2015).
- [36] V. V. Konotop, J. K. Yang, and D. A. Zezyulin, Nonlinear waves in  $\mathcal{PT}$ -symmetric systems, *Rev. Mod. Phys.* **88**, 035002 (2016).
- [37] S. V. Suchkov, A. A. Sukhorukov, J. H. Huang, S. V. Dmitriev, C. Lee, and Y. S. Kivshar, Nonlinear switching and solitons in  $\mathcal{PT}$ -symmetric photonic systems, *Laser Phot. Rev.* **10**, 177-213 (2016).
- [38] C. E. Rüter, K. G. Makris, R. El-Ganainy, D. N. Christodoulides, M. Segev, and D. Kip, Observation of parity-time symmetry in optics, *Nature Physics* **6**, 192-195 (2010).
- [39] D. V. Strunin and B. A. Malomed, Symmetry-breaking transitions in quiescent and moving solitons in fractional couplers, *Phys. Rev. E* **107**, 064203 (2023).
- [40] G. J. Milburn, J. Corney, E. M. Wright, and D. F. Walls, Quantum dynamics of an atomic Bose-Einstein condensate in a double-well potential, *Phys. Rev. A* **55**, 4318–4324 (1997).
- [41] A. Smerzi, S. Fantoni, S. Giovanazzi, and S. R. Shenoy, Quantum coherent atomic tunneling between two trapped Bose-Einstein condensates, *Phys. Rev. Lett.* **79**, 4950–4953 (1997).
- [42] J. Ruostekoski and D. F. Walls, Bose-Einstein condensate in a double-well potential as an open quantum system, *Phys. Rev. A* **58**, R50-R53 (1998).
- [43] S. Raghavan, A. Smerzi, S. Fantoni, S. R. Shenoy, Coherent oscillations between two weakly coupled Bose-Einstein condensates: Josephson effects,  $\pi$  oscillations, and macroscopic quantum self-trapping, *Phys. Rev. A* **59**, 620–633 (1999).
- [44] H. Sakaguchi and B. A. Malomed, Symmetry breaking of solitons in two-component Gross-Pitaevskii equations, *Phys. Rev. E* **83**, 036608 (2011).
- [45] H. Sakaguchi and B. A. Malomed, Symmetry breaking in a two-component system with repulsive interactions and linear coupling, *Comm. Nonlin. Sci. Num. Sim.* **92**, 105496 (2020).
- [46] M. Albiez, R. Gati, J. Fölling, S. Hunsmann, M. Cristiani, and M. K. Oberthaler, Direct observation of tunneling and nonlinear self-trapping in a single bosonic Josephson junction. *Phys. Rev. Lett.* **95**, 010402 (2005).
- [47] K. Kim, M.-S. Heo, K.-H. Lee, K. Jang, H.-R. Noh, D. Kim, and W. Jhe, Spontaneous Symmetry Breaking of Population between Two Dynamic Attractors in a Driven Atomic Trap: Ising-class Phase Transition, *Phys. Rev. Lett.* **96**, 150601 (2006).
- [48] A. Espinosa-Ceron, B. A. Malomed, J. Fujioka, and R. F. Rodriguez, Symmetry breaking in linearly coupled KdV systems, *Chaos* **22**, 033145 (2012).
- [49] T. Vicsek, A. Czirok, E. Ben-Jacob, I. Chen, and O. Shochet, Novel type of phase transition in a system of self-driven particles, *Phys. Rev. Lett.* **75**, 1226-1229 (1995).

- [50] M. Trippenbach, E. Infeld, J. Gocalek, M. Matuszewski, M. Oberthaler, and B. A. Malomed, Spontaneous symmetry breaking of gap solitons in double-well traps, *Phys. Rev. A* **78**, 013603 (2008).
- [51] X. Y. Zhang, J. L. Chai, D. Z. Ou, and Y. Y. Li, Antisymmetry breaking of discrete dipole gap solitons induced by a phase-slip defect, *Mod. Phys. Lett. B* **28**, 1450097 (2014).
- [52] S. Coleman and E. Weinberg, Radiative corrections as origin of spontaneous symmetry breaking, *Phys. Rev. D* **7**, 1888-1910 (1973).
- [53] L. Susskind, Dynamics of spontaneous symmetry breaking in the Weinberg-Salam theory, *Phys. Rev. D* **20**, 2619-2625 (1979).
- [54] F. Cooper, S. Habib, Y. Kluger, and E. Mottola, Nonequilibrium dynamics of symmetry breaking in  $\lambda\Phi^4$  theory, *Phys. Rev. D* **55**, 6471-6503 (1997).
- [55] G. C. Branco, P. M. Ferreira, L. Lavoura, M. N. Rebelo, M. Sher, and J. P. Silva, Theory and phenomenology of two-Higgs-doublet models, *Phys. Rep.* **516**, 1-102 (2012).
- [56] F. Englert and R. Brout, Broken symmetry and the mass of gauge vector mesons. *Phys. Rev. Lett.* **13**, 321-323 (1964).
- [57] P. W. Higgs, Broken symmetries and the masses of gauge bosons, *Phys. Rev. Lett.* **13**, 508-509 (1964).
- [58] G. S. Guralnik, C. R. Hagen, and T. W. B. Kibble, Global conservation laws and massless particles, *Phys. Rev. Lett.* **13**, 585-587 (1964).
- [59] J. Rossi, R. Carretero-González, P. G. Kevrekidis, and M. Haragus, On the spontaneous time-reversal symmetry breaking in synchronously-pumped passive Kerr resonators, *J. Phys. A Math. Theor.* **49**, 455201 (2016).
- [60] T. Mayteevarunyoo, B. A. Malomed, and G. Dong. Spontaneous symmetry breaking in a nonlinear double-well structure, *Phys. Rev. A* **78**, 053601 (2008).
- [61] X.-F. Zhou, S.-L. Zhang, Z.-W. Zhou, B. A. Malomed, and H. Pu, Bose-Einstein condensation on a ring-shaped trap with nonlinear double-well potential, *Phys. Rev. A* **85**, 023603 (2012).
- [62] B. A. Malomed and M. Ya. Azbel, Modulational instability of a wave scattered by a nonlinear center, *Phys. Rev. B* **47**, 10402-10406 (1993).
- [63] G. P. Agrawal, *Nonlinear Fiber Optics* (Academic Press, Amsterdam, 2013).
- [64] B. A. Malomed, Symmetry breaking in laser cavities, *Nature Phot.* **9**, 287-289 (2015).
- [65] E. Shamriz, N. Dror, and B. A. Malomed, Spontaneous symmetry breaking in a split potential box, *Phys. Rev. E* **94**, 022211 (2016).
- [66] G. Tempea and T. Brabec, Theory of self-focusing in a hollow waveguide, *Opt. Lett.* **23**, 762-764 (1998).
- [67] K. W. Oh, S. Choi, Y. M. Jung, and J. W. Lee, Novel hollow optical fibers and their applications in photonic devices for optical communications, *J. Lightwave Tech.* **23**, 524-532 (2005).
- [68] B. Debord, A. Amsanpally, M. Chafer, A. Baz, M. Maurel, J. M. Blondy, E. Hugonnot, F. Scol, L. Vincetti, F. G  r  me, and F. Benabid, Ultralow transmission loss in inhibited-coupling guiding hollow fibers, *Optica* **4**, 209-217 (2017).
- [69] A. L. Gaunt, T. F. Schmidutz, I. Gotlibovych, R. P. Smith, and Z. Hadzibabic, Bose-Einstein Condensation of Atoms in a Uniform Potential, *Phys. Rev. Lett.* **110**, 200406 (2013),
- [70] S. Gupta, K. W. Murch, K. L. Moore, T. P. Purdy, and D. M. Stamper-Kurn, Bose-Einstein Condensation in a Circular Waveguide, *Phys. Rev. Lett.* **95**, 143201 (2005).
- [71] C. Ryu, M. F. Andersen, P. Clad  , V. Natarajan, K. Helmerson, and W. D. Phillips, Observation of Persistent Flow of a Bose-Einstein Condensate in a Toroidal Trap, *Phys. Rev. Lett.* **99**, 260401 (2007).
- [72] B. E. Sherlock, M. Gildemeister, E. Owen, E. Nugent, and C. J. Foot, Time-averaged adiabatic ring potential for ultracold atoms, *Phys. Rev. A* **83**, 043408 (2011).
- [73] M. de Go  r de Herve, Y. Guo, C. De Rossi, A. Kumar, T. Badr, R. Dubessy, L. Longchambon, and H. Perrin, A versatile ring trap for quantum gases, *J. Phys. B: At. Mol. Opt. Phys.* **54**, 125302 (2021).
- [74] G. Iooss, and D. D. Joseph, *Elementary Stability and Bifurcation Theory* (Springer, New York, 1980).
- [75] J. D. Crawford and E. Knobloch, Symmetry and symmetry-breaking bifurcations in fluid dynamics, *Annual Rev. Fluid Mech.* **23**, 341-387 (1991).
- [76] P. G. Kevrekidis and D. J. Frantzeskakis, Pattern forming dynamical instabilities of Bose-Einstein condensates, *Mod. Phys. Lett. B* **18**, 173-202 (2004).
- [77] J. Laurie, U. Bortolozzo, S. Nazarenko, and S. Residori, One-dimensional optical wave turbulence: Experiment and theory, *Phys. Rep.* **514**, 121-175 (2012),
- [78] A. Ramanathan, K. C. Wright, S. R. Muniz, M. Zelan, W. T. Hill III, C. J. Lobb, K. Helmerson, W. D. Phillips, and G. K. Campbell, Superflow in a Toroidal Bose-Einstein Condensate: An Atom Circuit with a Tunable Weak Link, *Phys. Rev. Lett.* **106**, 130401 (2011).
- [79] D. Anderson, Variational approach to nonlinear pulse propagation in optical fibers, *Phys. Rev. A* **27**, 3135-3145 (1983).
- [80] B. A. Malomed, Variational methods in nonlinear fiber optics and related fields, *Prog. Optics* **43**, 71-193 (2002).
- [81] W. Z. Bao and Q. Du, Computing the ground state solution of Bose-Einstein condensates by a normalized gradient flow, *SIAM J. Sci. Comp.* **25**, 1674-1697 (2004).
- [82] J. T. Stuart and R. C. DiPrima, Eckhaus and Benjamin-Feir resonance mechanisms, *Proc. Roy. Soc. L. Ser. A – Math. Phys. Eng. Sci.* **362**, 27-41 (1978).
- [83] C. Kharif and E. Pelinovsky, Physical mechanisms of the rogue wave phenomenon, *Eur. J. Mech. B Fluids* **22**, 603-634 (2003).
- [84] A. Acus, B. A. Malomed, and Y. Shnir, Spontaneous symmetry breaking of binary fields in a nonlinear double-well structure, *Physica D* **241**, 987-1002 (2012).